Optical Properties of Au, Ag, and Bimetallic Au on Ag Nanohole Arrays

ARTICLE *in* THE JOURNAL OF PHYSICAL CHEMISTRY C · APRIL 2010

Impact Factor: 4.77 · DOI: 10.1021/jp101231c

Optical Properties of Au, Ag, and Bimetallic Au on Ag Nanohole Arrays

Marie-Pier Murray-Méthot,[†] Mathieu Ratel,[†] and Jean-Francois Masson*[,†,‡,§]

Département de Chimie, Université de Montréal, C. P. 6128 Succ. Centre-Ville, Montréal, Qc, Canada, H3C 3J7, Centre for Self-Assembled Chemical Structures (CSACS), and Centre for Biorecognition and Biosensors (CBB)

Received: February 8, 2010; Revised Manuscript Received: March 23, 2010

A systematic study of the optical properties and analytical response is reported for gold and silver nanohole arrays with different hole diameters with a fixed periodicity of 450 nm. Nanosphere lithography in combination with oxygen plasma etching has been used to fabricate the nanohole arrays. The plasmonic response of nanohole arrays is characterized in transmission spectroscopy ($\lambda = 500-1000$ nm spectral region), which varied with the metal composition and diameter of the nanoholes. The sensitivity to bulk refractive index (in nm/RIU) and the full width at half-maximum (FWHM) were measured for each plasmonic mode to compare the biosensing potential of the various nanohole arrays. A sensitivity of nearly 400 nm/RIU was observed and was maximal with the plasmonic band at $\lambda = 554$ nm for Ag nanohole arrays with the smallest hole diameter of 120 nm. Generally, the ratio of the full height (transmission intensity) and FWHM is constant for various hole diameters with Au nanohole arrays, whereas it improves for Ag nanohole arrays with smaller hole diameters. Various bimetallic nanohole arrays composed of a Ag underlayer covered with Au were fabricated with a hole diameter of 254 ± 20 nm and a depth of 50 ± 12 nm. Sensitivity and FH/FWHM ratio are improved for Au on Ag nanohole arrays compared with nanohole arrays of pure metal.

Introduction

Biosensors allow rapid and accurate detection of a specific bioanalyte, necessary for the detection of diseases. Recent advances in biosensors produced sensitive transducers, such as nanohole arrays.[1] Au and Ag nanohole arrays support a surface plasmon (SP), which can be excited in the visible range of the light spectrum, resulting in an enhanced transmission of light through the metallic film with subwavelength nanoholes. The wavelength of enhanced transmission at which the metal−solution interface is excited depends on the refractive index of a thin layer of solution near this interface. Thereby, the binding of biomolecules to the nanohole surface causes a red shift of the excitation wavelength due to their high refractive index. Of particular interest, the excitation of the SP in UV−vis by transmission spectroscopy could result in a miniature bioanalytical instrument due to the simple optical setup. These characteristics are primordial to building a portable biosensor. Moreover, the broad availability of a UV−vis spectrophotometer in most laboratories could also allow the implementation of nanohole array biosensors as a lab-based diagnostic tool. However, the use of nanohole arrays as a biosensor would benefit from higher sensitivity and lower detection limits for biomolecules. To better understand the effect of several physical/geometrical aspects on analytical parameters, a thorough study must be undertaken to develop optimal biosensors.

In recent years, research has been focusing on understanding the principles of enhanced transmission of light through nanohole arrays with a hole diameter smaller than the wavelength of light.[2−6] Others have reported the optical properties at a fixed periodicity and diameter of nanoholes.[3,4,6−9] In one example of a systematic study of optical properties/structure relationship, square arrays of nanoholes, concentric circles, and nanoslit arrays were characterized, finding similarities in the optical spectrum for wavelengths above $\lambda = 750$ nm for these structures.[4] However, nanohole arrays have evident differences for $\lambda < 750$ nm compared with concentric circles and nanoslits, as the optical response does not present the same plasmonic bands. The same study also investigated the variation of transmission spectra with several nanohole diameters, with a fixed periodicity of 600 nm. It was shown that strong differences exist in the optical properties of these nanohole arrays.[4] Theoretical simulations provide a tool to predict optical properties of nanohole arrays. Finite difference−time domain (FDTD) simulations of light transmitting through isolated nanoholes or arrays provide the assignment of the plasmonic bands.[2,5] Parsons et al. reported that a good correlation exists between experimental and simulated transmission spectra of Au nanohole arrays with identical diameters and depths.[6] They also observed a red shift of the (1,0) metal-solution resonance band by increasing the period of the nanohole array.[6] For nanohole arrays, the (i,j) nomenclature refers to an orientation parameter of the array (Figure 1). Multiple resonances are excited for the various orientation parameters and for the various interfaces (i.e., metal−glass and metal−solution) present in nanohole arrays. Optical properties of nanohole arrays are, therefore, highly influenced by the physical and geometrical parameters of the array.

The refractive index sensitivity of plasmonic materials is an important parameter in assessing the analytical potential of the material in a biosensor format. It was reported that the periodicity, the integers of the Bloch modes, and the metal composition are factors influencing the sensitivity.[10] Other factors, such as the hole diameter, can also influence sensitivity.[4] A survey of the literature shows that the sensitivity for disordered nanohole arrays typically ranges from 40 to 270 nm/RIU, whereas ordered nanohole arrays exhibit a sensitivity from 200 nm/RIU for a periodicity of 400 to 1570 nm/RIU for a

* To whom correspondence should be addressed. Tel: 1-514-343-7342. Fax: 1-514-343-7586. E-mail: jf.masson@umontreal.ca.
† Université de Montréal.
‡ Centre for Self-Assembled Chemical Structures (CSACS).
§ Centre for Biorecognition and Biosensors (CBB).

10.1021/jp101231c
Published on Web 04/14/2010

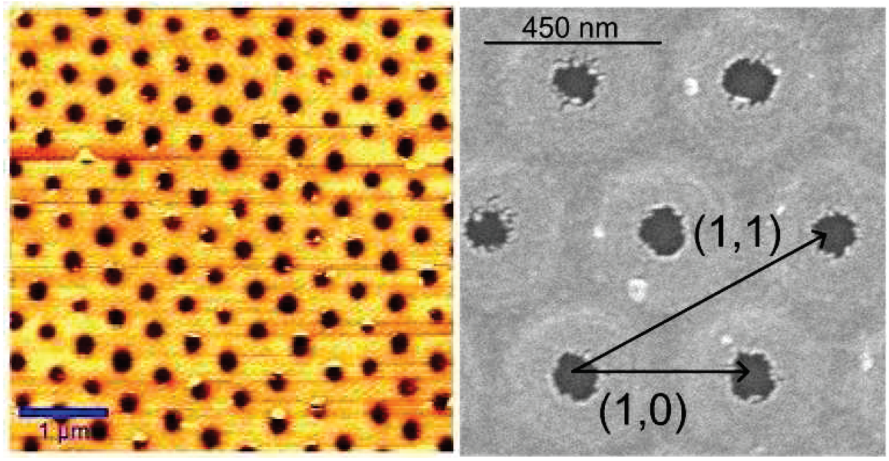

Figure 1. (left) AFM image of a nanohole array with a periodicity of 450 nm with a diameter of 195 ± 19 nm. (right) SEM image of a nanohole array demonstrating the (*i*,*j*) nomenclature and the irregular edges of each nanohole.

TABLE 1: Sensitivity of Nanohole Arrays with Different Geometries

periodicity (nm)	geometry	diameter (nm)	depth (nm)	metal	overlayer	sensitivity (nm/RIU)	ref
	disordered	60	20	Au	none	71−88	49
	disordered	140	15−30	Au or Ag	none or 20 nm SiO_x	75−270	50, 51
	disordered	110	55	Au	none	40−60	52
400	square array	100	50	Au	none	200	5
450	square array	150	100	Au	none	333	53
500	square array	NA[a]	100	Au	none	324	54
500	square array	170	100	Au	50 nm SiO_x	650	1
600	square array	90−250	110	Au	none	420 and 561	4
600	square array of double holes	200	100	Au	none	270 and 600	55
1530	square array	300	150−200	Au	none	1570 and 1110	10, 14
450	hexagonal array	250	7−13	Au	none	154−487	24
450	hexagonal array	320	48	Au	none	226	24

[a] NA: data not available.

periodicity of 1.53 μm (Table 1). However, these reports are mostly for nanohole arrays of a single geometry, almost exclusively for Au, and no complete investigation of the sensitivity of nanohole arrays is available for series of nanoholes. Another important parameter to investigate is the sensitivity to monolayer formation and for the detection of biomolecules. In a biosensing experiment, a wavelength shift of 10 nm was observed for the binding of streptavidin on biotin immobilized on nanohole arrays.[1] The normalized transmission intensity can also be used for biosensing with shifts of 0.2 au for the biotin and streptavidin interaction.[11] A biosensor was developed based on nanohole arrays incorporated in a microfluidic chip and successfully detected the binding of mercaptoundecanoic acid on the nanohole arrays with a shift of 9 nm.[12,13] Several applications of biosensors using nanohole arrays were developed for the detection of BSA,[10,14−16] IgG,[17] and glutathione S-transferase (GST).[18] These examples show the general analytical properties of nanohole arrays.

Nanohole arrays with subwavelength nanoholes can be fabricated with high-resolution techniques, such as electron beam lithography[4,19] or focused ion beam.[6,20] These techniques allow an excellent control of the size and shape of the nanohole arrays. Soft embossing lithography is an alternative technique for the fabrication of larger areas of well-ordered nanohole arrays.[21,22] However, different masks must be fabricated with significant cost for modifying the physical aspect of the nanohole arrays. The manufacture of series of nanohole arrays with various physical aspects would be beneficial for the investigation of the periodicity and hole diameter effect on the analytical properties. To achieve this objective, nanosphere lithography (NSL) is a rapid and inexpensive technique to fabricate arrays of nanoparticles, where self-assembled polystyrene nanospheres are arranged in close-packed hexagonal arrays.[23] Nanohole arrays can be obtained with this NSL mask from the electrochemical deposition of a metal layer in the voids created by the mask.[23] Moreover, nanohole arrays can be obtained from glancing angle deposition (GLAD) of a metal layer at a 27° angle on the NSL mask with a planetary rotation stage.[24] However, these techniques do not allow the control of the hole diameter and have limited range for the depth of the nanoholes. Alternatively, reactive ion etching (RIE) with oxygen plasma has been recently used to decrease the diameter of the nanosphere immobilized to a substrate, in order to obtain a hexagonal array of nonclosed-packed spheres.[24−32] The etching step controls the diameter of the nanosphere without significantly altering the periodicity of the crystalline lattice. Deposition of metal at an angle normal to the surface, followed by the removal of the nanospheres, results in nanohole arrays. Using this methodology, the periodicity is equal to the initial nanosphere diameter, and the nanohole diameter is identical to the size of the etched nanosphere, which can be as small as 30 nm.[27] Thereby, NSL in combination with RIE is an excellent tool to fabricate the numerous nanohole arrays necessary to investigate their optical properties.

Experimental Section

Nanosphere Mask. The technique to organize the latex nanospheres on a glass slide was based on prior reports.[24,33,34] Glass slides were immersed in a piranha solution composed of 75% sulphuric acid and 25% hydrogen peroxide for 90 min.

Caution: piranha solution is very corrosive. The glass slides were then rinsed with plenty of 18 MΩ water and sonicated in 18 MΩ water to remove traces of piranha solution. Thereafter, they were immersed in a 5:1:1 solution of 18 MΩ water/H_2O_2/ammonium hydroxide and sonicated for 60 min. Finally, they were rinsed with plenty of 18 MΩ water and sonicated numerous times in 18 MΩ water. The cleaned glass slides were stored in ultrapure water for weeks, which was replaced three times per week. The nanosphere solution was prepared by mixing 30 μL of ethanol with 30 μL of a 10% solution of 450 ± 15 nm latex nanospheres (Duke Scientific, now Thermo Fisher particle technology). The latex nanospheres were stored at 4 °C, so the diluted nanosphere solution had to be stabilized for 2 h at room temperature before use. A 10 μL aliquot of the diluted nanosphere solution was deposited on a dry glass slide that was promptly transferred on the positive meniscus of water in a 6 cm Petri dish. The nanospheres at the water surface were transferred on a clean and wet coverslip by the Langmuir−Blodgett technique. The nanosphere mask was dried under a Petri dish for several hours prior to subsequent preparation steps.

Control of the Nanosphere Diameter. Oxygen plasma treatment was used to control the diameter of the nanospheres. A plasma cleaner (Harrick Plasma Cleaner PDC-32G) was used at high power (18 W) from 0 min (for unetched samples) to 10 min (for smallest nanoholes). Prior to the etching process, a vacuum was performed for 20 min with an oxygen flow of 15 mL/min in the plasma chamber, which was maintained during the etching process. Thereafter, a Ag or Au film (ESPI metals, purity > 99.95%) was deposited on the etched nanosphere mask using a Cressington 308R sputter coating system, with a thickness controller and a 100 W sputter supply. A 5 nm Ti layer was deposited to increase the adhesion of the 45 nm thick Au layer to the glass slide. Fifty nanometers of Ag was deposited as Ag adheres well to glass. The nanosphere mask was then removed by sonication in ethanol. The nanohole arrays obtained were physically characterized by AFM contact mode (Witec Atomic Force microscope alpha300A) and by SEM (Hitachi S-4700).

Optical Properties Measurement. The nanohole arrays were glued with an optical-grade UV epoxy on a 1-cm wide microscope glass slide for better handling and insertion into a standard UV−vis cuvette. The optical characterization was performed in transmission spectroscopy with a custom optical setup using a fiber optic spectrometer coupled with a CCD camera within a working range of $\lambda = 360-1000$ nm. A halogen lamp with an emission range of $\lambda = 400-1200$ nm was collimated and impinged on the nanohole arrays at a 0° angle from the surface of the nanoholes. Using this configuration, the light beam impinges perpendicular to the plane of the nanohole film. The sensitivity was measured from 1.33 to 1.41 RIU with aqueous sucrose solutions (0−50% w/w) to vary the refractive index of the medium in contact with the nanohole array. The transmission spectra were then analyzed with MatLab. The spectral position of the excitation wavelength for the maximum or minimum of transmission (depending on the spectral band) was obtained using the zero of the first derivative of the peak. The full height/full width at half-maximum ratio (FH/FWHM) was measured with the closest inflection point. It is also important to note that each result reports the average value from at least three independent nanohole arrays, while the error reports two standard deviations about the mean.

Results and Discussion

Optical Properties of Ag and Au Nanohole Arrays. Biosensors can be constructed based on the plasmonic properties of metal. Surface plasmons can detect changes of refractive index near the surface, related to the adsorption of biomolecules. In particular, the LSPR properties of nanoparticles have been exploited to detect biomolecules.[35] Nanohole arrays can exhibit greater sensitivity to refractive index (Table 1) than nanoparticles (235 nm/RIU).[36] The interest to develop nanohole arrays is driven by this possibility of sensors with greater sensitivity. Numerous parameters can be tuned to develop nanohole arrays with optimal analytical properties. Sensitivity to refractive index increases the change of wavelength for a binding event, and a sharp and intense plasmonic band maximizes resolution. Although numerous studies report the optical properties of nanohole arrays, it is usually for a fixed periodicity, geometry, hole diameter, and unique metal composition. In prior reports, Au was almost exclusively investigated (Table 1). Hence, the optical properties of nanohole arrays are studied here with various hole diameters and metal compositions.

Nanohole arrays were prepared with a modified nanosphere lithography technique, with the advantage of the simple modification of the nanosphere mask diameter with oxygen plasma. The periodicity was set at 450 nm (the process is not limited to this periodicity) with latex nanospheres of the same size. The oxygen plasma process controls the size of the latex nanospheres from the initial diameter to 120 nm. Figure 1 (left panel) shows a nanohole array with a periodicity of 450 nm, a hole diameter of 195 ± 19 nm, and a depth of 53 ± 8 nm. AFM images were acquired to determine the depth of the holes, whereas SEM provided better resolution for the diameter of the nanoholes. The SEM images had previously demonstrated that etching the nanosphere mask does not alter the periodicity of the nanohole arrays, although the roughness of the nanosphere increases with longer etch time.[30] Hence, the nanosphere roughness results in nanoholes with somewhat irregular edges (Figure 1, right panel), especially for smaller nanohole diameters.

The AFM images showed residues left on the surface of the nanohole arrays. This can be caused by metal fragments from the nanosphere capped with Au or Ag or from residual polymer of the nanosphere. The residue was also visible on microhole arrays prepared using the same methodology.[37] The residues are covering a very small fraction of the surface, such that the plasmonic response should be minimally altered, if it is altered. The small deviation on the optical response (excitation wavelength; see below) suggests that the residue has a minimal effect on the plasmonic response. One drawback of NSL followed by RIE is that the latex spheres are not fully removed for longer etching time. This is likely due to a strong contact point between the metal layer on the latex sphere and the metal film deposited on the glass slide. This strong contact point may prohibit the complete removal of the smaller nanospheres using ultrasounds. Numerous unsuccessful attempts were made with mechanical vibrations and wet polishing techniques to remove the nanosphere mask for longer etch times. Polishing with 0.05 μm alumina provided partial removal of the nanosphere mask, but many scratches were observed, which limited this technique. This factor restricted the nanohole diameter range in this study to ≥180 nm for Au and ≥120 nm for Ag. Nanospheres mainly remained on the surface with nanohole arrays with hole diameters smaller than these diameters. As an example, nearly 45% of the spheres remained on the surface with Au nanohole arrays with a diameter of 180 nm, 35% for holes with a diameter of 205 nm, 13% for holes with a diameter of 220 nm, and 0%

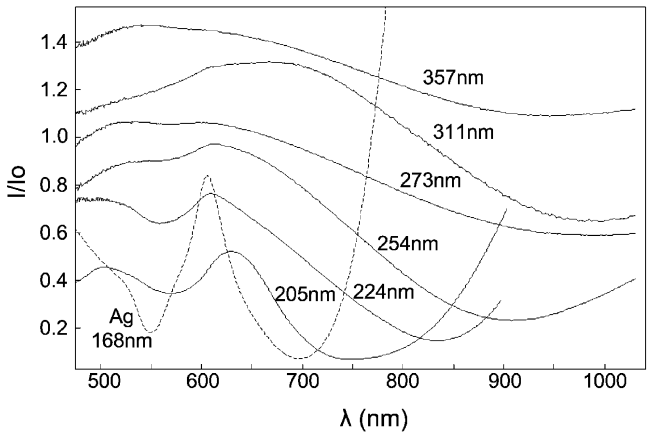

Figure 2. Transmission spectra for Au (lines) and Ag (dashed) nanohole arrays with different nanohole diameters. For diameters between 300 and 450 nm, there is only one minimum of transmission, characteristic of the LSPR response in triangle arrays. For nanohole diameters below 300 nm, a maximum (near 600 nm) and a minimum (near 550 nm) of transmission appear in the transmission spectra. The curves are offset for ease of representation. The plasmonic band positions for Ag are blue shifted compared with the Au band.

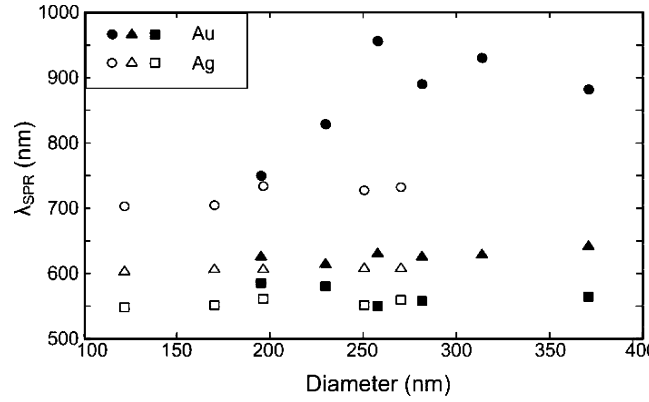

Figure 3. Resonant wavelength for each plasmonic band for Au (filled) and Ag (open) nanohole arrays. The squares represent the transmission minimum associated with the (1,0) solution−metal plasmonic band, the diamonds are associated with the enhanced transmission maximum for the (1,0) metal−glass interface, and the circles relate to the minimum of transmission in the near-infrared.

for holes with a diameter of 250 nm. For Ag nanohole arrays, nanospheres were fully removed for every sample up to 120 nm in diameter. For both Ag and Au nanohole arrays, for diameters smaller than 180 nm for Au and 120 nm for Ag, 100% of spheres remained on the surface. The samples with partially removed nanospheres still exhibited a plasmonic response. The optical response showed identical plasmonic bands, but of decreased intensity. Samples with hole diameters larger than 180 nm for Au and 120 nm for Ag showed nearly complete removal of the spheres (as demonstrated by the AFM image in Figure 1). However, it still provides a broad range of nanohole diameters and does not prohibit the use of modified nanosphere lithography.

The optical characterization of different nanohole diameters was accomplished with various analytical parameters: the excitation wavelength of the plasmonic bands, the FH/FWHM ratio, and the sensitivity to bulk refractive index change. The evolution of the spectra with decreasing Au nanohole diameter is presented in Figure 2. For Ag arrays, the optical response is similar, with the exception that the plasmonic peaks are more intense and blue shifted. The optical spectrum of Au nanohole arrays reveals the presence of a transmission minimum in the near-infrared (NIR) for every hole diameter. The position of this transmission minimum varies significantly, depending on the diameter of the hole. The excitation wavelength of the NIR plasmonic band is red shifted for larger nanohole diameters of Au nanohole arrays (Figure 3). For smaller hole diameters, the transmission band is excited near $\lambda = 750$ nm and the plasmonic wavelength increases with diameter to reach a plateau near $\lambda = 900$ nm for diameters above 250 nm. A transmission maximum appears as the diameter decreases, at an average wavelength of 641 ± 20 nm. The intensity of this plasmonic band generally increases as the diameter decreases. This enhanced transmission band was previously associated with the (1,0) metal−glass plasmon resonance.[5,26] For smaller diameters (diameter < 300 nm), a second transmission minimum is observed at an average wavelength of 563 ± 11 nm, associated with the (1,0) metal−solution interface,[5,26] as well as a second transmission maximum at $\lambda = 534 \pm 31$ nm, associated with the (1,1) metal−glass interface. The positions of these plasmonic bands, (1,0) metal−glass and (1,0) metal−solution, do not show any significant changes in excitation wavelength with different diameters (Figure 3). The minute variations of the excitation wavelengths for these plasmonic peaks are not significant.

Comparison of the different spectra for Ag nanohole arrays results in similar optical properties than Au nanohole arrays. Two transmission minima were observed, one in the NIR at $\lambda = 722 \pm 30$ nm and another associated with the (1,0) metal−solution interface at $\lambda = 554 \pm 9$ nm. A transmission maximum is also present at $\lambda = 606 \pm 2$ nm in Ag nanohole arrays, related to the (1,0) glass−Ag interface. In all cases, the Ag plasmonic bands are blue shifted compared with the gold plasmonic band, for identical solutions and physical parameters (Figure 3). The different complex dielectric constants of Ag result in plasmonic bands active at lower wavelength for SPR.[38] Each plasmonic band for Ag nanohole arrays does not shift significantly with varying hole diameter. However, for both Au and Ag nanohole arrays, it is observed that the intensity of the plasmonic peak is significantly modified by the diameter of the nanoholes. Generally, the plasmonic peaks become more intense with decreasing the nanohole diameter. This important factor is related to the precision at which the position of the minimum can be determined. Peaks of greater intensity result in more precise tracking of the plasmonic wavelength, which translates into greater resolution.

Sensitivity for Ag and Au Nanohole Arrays. Nanohole arrays could potentially be used into biosensor schemes.[20,39] The sensitivity to refractive index must be maximal for improved biosensing capability. This is measured from the wavelength shift with the variation of the refractive index (nm/RIU) of the solution in contact with the nanohole arrays. Different concentrations of aqueous sucrose solutions were used to vary the refractive index at the metal−solution interface from 1.33 to 1.41 RIU. Figure 4 reports the transmission spectra of a silver nanohole array for different refractive index solutions at the metal interface. For this example, the nanohole array has a periodicity of 450 nm, a nanohole diameter of 255 ± 16 nm, and a depth of 50 ± 11 nm. It is possible to observe the minimum of transmission associated with the (1,0) metal−solution interface in the spectral range from $\lambda = 520$ to 590 nm for aqueous solutions of glucose and at $\lambda = 419$ nm in air. There is a red shift of the minimum position for a refractive index increase of the solution, resulting in a sensitivity greater than 200 nm/RIU for every nanohole diameter of Ag arrays. This sensitivity increases with smaller hole diameters to nearly 400

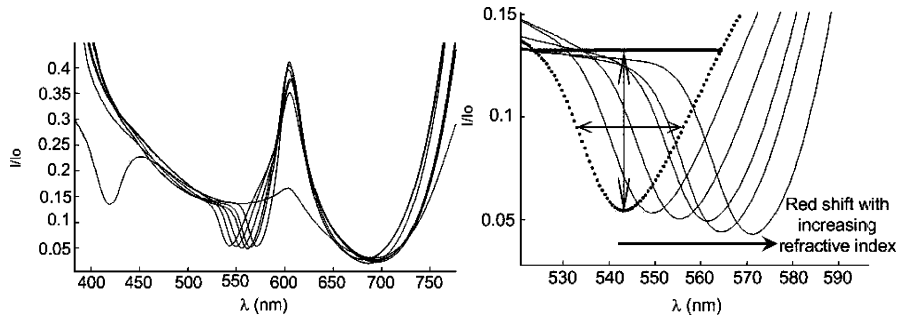

Figure 4. (left) Transmission spectra of a Ag nanohole array with a periodicity of 450 nm, a nanohole diameter of 255 ± 16, and a depth of 50 ± 11 nm. (right) The spectral range from $\lambda = 520$ to 590 nm shows the refractive index sensitivity and the method for calculating the FH/FWHM. The vertical arrow indicates the FH, whereas the horizontal arrow is for the FWHM.

nm/RIU. For Au arrays, the (1,0) metal−solution plasmonic band has a constant sensitivity of 204 ± 48 nm/RIU, regardless of the hole diameter. The sensitivity of the minima associated with the (1,0) metal−solution at $\lambda = 563$ nm for Au and $\lambda = 554$ nm for Ag is the most sensitive peak for nanohole arrays with a periodicity of 450 nm. This observation is only valid for nanohole diameters < 300 nm, as the (1,0) metal−solution plasmonic band is nonexistent for larger diameters. Thus, the peak of interest in a biosensing scheme is the (1,0) metal−solution band active around $\lambda = 540-570$ nm.

A theoretical analysis reported that the sensitivity was proportional to the periodicity, the Bloch modes, and the dielectric constant of the metal and solution.[10] This would explain the constant sensitivity for Au, with hole diameters greater than 180 nm. In the case of Ag nanohole arrays, we do observe that the sensitivity increases significantly for smaller hole diameters (Figure 5). However, Lee et al. recently reported that the sensitivity increases for Au nanoholes from 220 to 90 nm in hole diameter, with a 600 nm periodicity.[4] Although we could not measure the sensitivity in this region of nanohole sizes with Au, we did observe that the sensitivity increased for Ag nanoholes for smaller hole diameters. However, it suggests that theoretical modeling should be adapted to account for the variation of sensitivity with smaller hole diameters.

The other plasmonic bands active in Au or Ag nanohole arrays are significantly less sensitive to refractive index. For the minimum at $\lambda = 722$ nm in Ag nanohole arrays, the sensitivity measured was negative with an average value of −137 ± 74 nm/RIU. In that case, an increase of refractive index results in a blue shift of the minimum of transmission. The sensitivity of this plasmonic band does not significantly change for the different hole diameters. Moreover, the error associated with the sensitivity is rather large due to a spectrally broad response decreasing the accuracy of the measurement. The minimum of transmission for Au nanohole arrays at $\lambda = 882$ nm is less sensitive than for the minimum around $\lambda = 540-570$ nm, with a sensitivity of 154 ± 26 nm/RIU. In that case, the sensitivity is positive; thus, a red shift is observed for increasing refractive index. The sensitivity for Au nanohole arrays is stable with various nanohole diameters. The maximum of transmission near $\lambda = 600$ nm is relatively insensitive to refractive index. The plasmonic band exhibits only a weak red shift for a refractive index increase. The average sensitivity is 91 ± 39 nm/RIU for Au arrays and 34 ± 17 nm/RIU for Ag arrays. This band was not as sensitive as the other two transmission minima reported above for Au and Ag nanohole arrays. This result is expected because the low sensitivity plasmonic band is associated with the (1,0) glass−metal interface and should not be sensitive to the bulk refractive index.

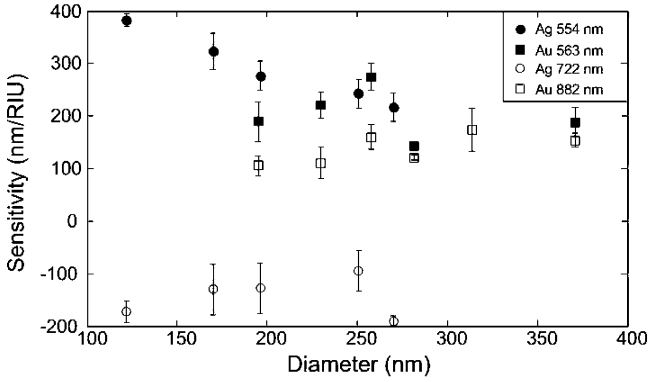

Figure 5. Sensitivity of nanohole arrays with different diameters is shown for Ag (circles) and Au (squares) nanohole arrays. Sensitivity is generally higher for the plasmonic bands near $\lambda = 550$ nm (filled forms) for Ag and Au, whereas it also increases for Ag nanoholes with decreasing diameters.

FH/FWHM for Ag and Au Nanohole Arrays. The resolution of spectroscopic techniques is improved for narrow and intense absorption or transmission bands. A measure of sharpness and intensity of plasmonic bands can be obtained from the ratio of the full height (FH, related to the intensity) divided by the full width at half-maximum (FWHM, related to the sharpness of the band or the line width). A large FH/FWHM value signifies that the plasmonic peak has better spectral resolution. This figure of merit provides a methodology to compare the sharpness and intensity of the various plasmonic bands observed in nanohole arrays. As an example, considering only the line width does not account for the intensity of a plasmonic band, which greatly varies for nanohole arrays of different geometries and for the various plasmonic bands active in nanohole arrays. The line width is an appropriate figure of merit for nanotriangle arrays, as the intensity of the unique plasmonic band is usually normalized. In all cases, the height was measured for the nanohole arrays in water, as described in Figure 4 (right panel). This method provides a good estimation of the accuracy at which the plasmonic wavelength can be measured. Greater accuracy on the measurement of the plasmonic wavelength provides better RI resolution.

With the larger nanoholes, the transmission spectra of Au and Ag nanohole arrays are dominated by the absorption band due to the LSPR similar to individual triangles. As the nanohole diameter decreases, the spectra exhibit new plasmonic peaks. Because the only peak of significant sensitivity for nanohole arrays was for the (1,0) metal−solution interface, only this peak is considered in this section. Figure 6 shows the variation of FH/FWHM with the diameter of the nanoholes for the Ag and

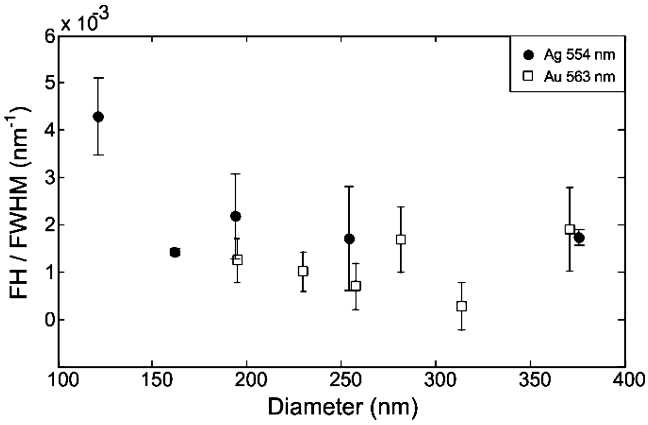

Figure 6. Variation of the FH/FWHM ratio of the minimum of transmission of the (1,0) solution−metal plasmonic band at $\lambda = 554$ nm for Ag arrays (filled circles) and at $\lambda = 563$ nm for Au arrays (squares). This value has to be maximal to improve resolution.

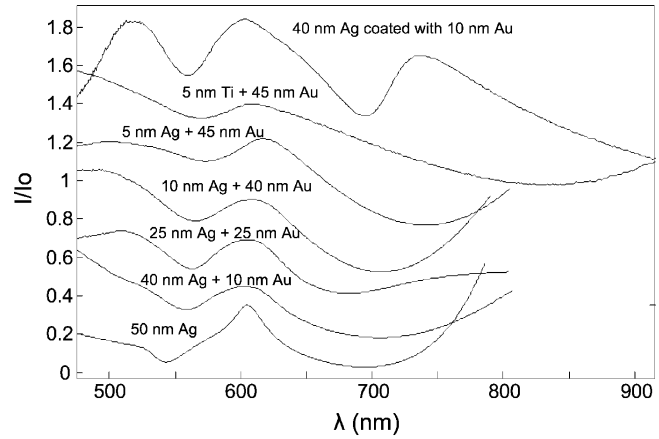

Figure 7. Transmission spectra of nanohole arrays with different thicknesses of Ag and Au. The periodicity is 450 nm, and the nanohole diameter is 254 ± 20 nm. The total nanohole depth is 50 ± 12 nm, with various thicknesses of Ag and Au. Ag is used as the underlayer, while Au is exposed to the solution. The 40 nm of Ag coated with 10 nm of Au refers to a Ag nanohole array fully coated with 10 nm of Au.

Au nanohole arrays. The FH/FWHM ratio is relatively constant for Au arrays, around 1×10^{-3} nm^{-1}. However, the FH/FWHM ratio is increasing as the diameter decreases for Ag nanohole arrays from around 2×10^{-3} to 4×10^{-3} nm^{-1}. This increase in the FH/FWHM ratio is a result of the increase in intensity of the plasmonic peak. The transmission minimum ($\lambda = 540-570$ nm) is of weak intensity for larger diameters, which increases for smaller nanohole diameters. The FH/FWHM ratio is twice better for Ag nanoholes with diameters of 120 ± 10 nm than for other Au and Ag nanohole arrays. Thus, a smaller hole diameter for Ag nanohole arrays provides better sensitivity and a better FH/FWHM ratio.

Bimetallic Au on Ag Nanohole Arrays. Ag surfaces can be oxidized, which could limit the shelf time of Ag nanohole arrays. SPR sensors based on unprotected Ag films are usually stable for less than 1 month, although depositing a self-assembled monolayer can increase the shelf life.[40] Ag provides desirable analytical properties for nanohole arrays, as described above. Thus, one alternative investigated herein has been the possibility of using Ag as an undercoat with Au protecting the surface. Hence, the nanohole array could have the spectral characteristics of Ag nanohole arrays combined with the stability of Au to oxidation. Moreover, the Au surface is advantageous for the increased stability of thiol chemistry.[41] Bimetallic nanohole arrays were prepared by depositing a Au film on the Ag film prior to the removal of the NSL mask. In this series of nanohole arrays, the depth was maintained constant at 50 ± 12 nm, but with different thicknesses of Ag (5−50 nm) and Au (45−0 nm). The diameter of the nanoholes was 254 ± 20 nm. Figure 7 shows the transmission spectra for these nanohole arrays. It is possible to observe the (1,0) metal−solution band shift toward lower wavelengths as the thickness of the silver layer increases (Table 1). The nanohole arrays with the thinnest Ag layers are active around $\lambda = 570$ nm, which decreases to $\lambda = 551$ nm for pure Ag nanohole arrays. It was previously demonstrated that the excitation wavelength was a function of the dielectric constant of the metal layer.[42] Ag has a lower dielectric constant than that of Au in the visible spectral region[38] and, thus, results in a shorter excitation wavelength for Ag compared with Au. The excitation wavelength for the (1,0) metal−solution interface for the nanohole arrays with 5 nm of Ti and 45 nm o Au is blue shifted compared with 5 nm of Ag and 45 nm of Au. Moreover, the transmission minimum in the NIR is significantly red shifted for the 5 nm of Ti with 45 nm of Au. These shifts of the plasmonic bands are due to the different dielectric constants of Ag and Ti, changing the propagation properties of the surface plasmon wave in the nanohole film and the excitation wavelength. Hence, the optical spectrum of bimetallic Au on Ag nanohole arrays is similar to the pure metal nanohole arrays, with differences in the position of the plasmonic bands, depending on the metal undercoat.

The sensitivity of these bimetallic Ag/Au nanohole arrays does not vary significantly for most of the bimetallic materials. The sensitivity ranges from 242 to 303 nm/RIU, which is maximal for 10 nm of Ag and 40 nm of Au (Table 2). For other metal compositions, it is relatively constant between 242 and 269 nm/RIU. Similar to the sensitivity, the FH/FWHM ratio is dependent on the metal composition. Despite the band becoming narrower for increased Ag thickness (line width around 38 nm for Au and 28 nm for Ag), the nanohole with 50 nm of Ag does not provide the best FH/FWHM ratio due to the decrease in intensity of the band for the thicker Ag layer compared with bimetallic Au on Ag. The FH/FWHM ratio of the plasmonic peaks is optimal with 25 nm of Ag and Au (Table 2). For other metal compositions, the FH/FWHM ratio decreases.

These results indicate that the excitation wavelength, the sensitivity, and the FH/FWHM ratio of bimetallic Au on Ag nanohole arrays are dependent on the metal composition of the nanohole arrays, and the optical properties of bimetallic Au on Ag nanoholes are improved compared with the pure metal nanohole arrays. Comparatively, the excitation wavelength for bimetallic Au/Ag nanoparticles has been observed to shift from the excitation wavelength of pure Au to the one of pure Ag. The shift was proportional to the fraction of Au and Ag present in the nanoparticle.[43,44] This result for bimetallic nanoparticles is in accordance with the shift of wavelength observed here for the Au on Ag nanohole arrays from $\lambda = 570$ nm for Au to $\lambda = 551$ nm for Ag. It has also been reported that the effective dielectric constant of bimetallic nanoparticles is not a linear combination of the one from pure metals.[43] This effect may be linked to the coupling of the surface plasmons of the two metal layers.[45] Using conventional surface plasmon resonance, it was demonstrated that the line width of the SPR resonance decreased from Au to Ag, proportionally to the fraction of each metal composing the thin film.[46] In the case of nanohole arrays, it was observed that the line width for Au is indeed larger than that for Ag, but no correlation was observed for the intermediate

TABLE 2: Analytical Parameters for Bimetallic Au on Ag Nanoholes

thickness (nm)	50 Ag	40 Ag 10 Au	25 Ag 25 Au	10 Ag 40 Au	5 Ag 45 Au	5 Ti 45 Au	Au-coated Ag arrays	optimal Ag[a]	mean values Au[b]
λ (nm)	551	559	564	567	572	569	565	547	563
sensitivity (nm/RIU)	242 ± 46	267 ± 71	269 ± 37	303 ± 6	253 ± 48	252 ± 36	210 ± 78	383 ± 23	204 ± 48
FH/FWHM (10^{-3} nm^{-1})	2 ± 1	2.4 ± 0.6	9 ± 2	4 ± 3	2.0 ± 0.3	1.13 ± 0.04	2.0 ± 0.4	4.3 ± 0.8	1.2 ± 0.8

[a] Optimal Ag nanohole diameter of 122 ± 10 nm. [b] Mean values for all Au nanohole diameters.

composition of Ag and Au. However, it was observed that the FH/FWHM is better for Ag than for Au but also improves significantly for bimetallic layers. This may be explained by the increase in intensity of the plasmonic response for nanohole arrays (Au on Ag). A similar effect was observed and predicted using the Mie theory for core−shell Au and Ag nanoparticles.[47] As the number of shells increased, the intensity of the absorption increased dramatically. Thereby, the optical properties of Au on Ag nanohole arrays are similar to those of bimetallic nanoparticles.

A different configuration of Au on Ag nanohole arrays was also investigated. A series of nanohole arrays with 40 nm of Ag were prepared. Following the removal of the NSL mask, a 10 nm overlayer of Au was deposited, thus coating not only the Ag layer but also the glass surface of the nanoholes. The result is a Ag nanohole array coated with 10 nm of Au, with nanoholes 40 nm in depth. Two major differences emerge by comparing the optical spectrum of the Au-coated Ag nanohole array with the 40 nm of Ag + 10 nm of Au nanohole array (Figure 7). First, an additional lower energy resonance is observed for the Au-coated Ag nanohole array (λ = 742 nm). Moreover, the intensity of the plasmonic peaks is increased significantly for every plasmonic band. One example is the maximum at λ = 519 nm for the (1,1) metal−glass band, hardly observed for Au and Ag nanoholes with diameters < 250 nm. This band is much stronger for the Au-coated Ag nanohole array. Also, the maximum at λ = 742 nm observed for the Au-coated Ag nanoholes is not present in any other nanoholes prepared herein. This is likely to be due to an enhanced transmission created by the thin gold metal layer in the nanoholes, as it was not observed for the nanohole array with glass at the bottom of the nanohole. In comparison, this spectrum is very similar to the Au nanohole arrays capped with Au disks prepared by the Nuzzo group, where an increased number of resonance bands are present, compared with other nanohole arrays.[48] The resonance at lower energy was attributed to the plasmon coupling between the upper ring of the nanohole to the metallic surface at the bottom of the nanohole. This could be the case with the Au-coated Ag nanoholes prepared here. However, the sensitivity and the FH/FWHM are not improved with the Au-coated Ag nanohole arrays compared to other bimetallic nanohole arrays.

Conclusions

The optical and analytical properties of nanohole arrays can be tuned by modifying the diameter of the nanohole and the metal composition. The sensitivity and FH/FWHM ratio are improved for Ag nanohole arrays with smaller hole diameters compared with other Ag nanohole arrays and Au nanohole arrays. This is obtained with the (1,0) metal−solution plasmonic band, excited at λ = 540−570 nm for nanohole arrays with a periodicity of 450 nm. Other plasmonic peaks exhibited analytical parameters of decreased performances, such that they could not be used in biosensing. A bimetallic metallic composition using Ag as the adhesion layer and Au as the top layer improves the sensitivity and the FH/FWHM ratio compared with pure Ag or Au nanohole arrays. These bimetallic nanohole arrays are, therefore, interesting plasmonic materials for biosensing.

Acknowledgment. Financial support was provided by Nano-Québec, the Canadian Space Agency, the Canadian Foundation for Innovation (CFI), and the National Sciences and Engineering Research Council of Canada (NSERC).

References and Notes

(1) Ferreira, J.; Santos, M. J. L.; Rahman, M. M.; Brolo, A. G.; Gordon, R.; Sinton, D.; Girotto, E. M. *J. Am. Chem. Soc.* **2009**, *131*, 436–437.
(2) Chang, S. H.; Gray, S. K.; Schatz, G. C. *Opt. Express* **2005**, *13*, 3150–3165.
(3) Ebbesen, T. W.; Lezec, H. J.; Ghaemi, H. F.; Thio, T.; Wolff, P. A. *Nature* **1998**, *391*, 667–669.
(4) Lee, K. L.; Wang, W. S.; Wei, P. K. *Plasmonics* **2008**, *3*, 119–125.
(5) McMahon, J. M.; Henzie, J.; Odom, T. W.; Schatz, G. C.; Gray, S. K. *Opt. Express* **2007**, *15*, 18119–18129.
(6) Parsons, J.; Hendry, E.; Burrows, C. P.; Auguie, B.; Sambles, J. R.; Barnes, W. L. *Phys. Rev. B* **2009**, *79*, 073412.
(7) Canpean, V.; Astilean, S. *Mater. Lett.* **2009**, *63*, 2520–2522.
(8) Genet, C.; Ebbesen, T. W. *Nature* **2007**, *445*, 39–46.
(9) Jensen, T. R.; Malinsky, M. D.; Haynes, C. L.; Van Duyne, R. P. *J. Phys. Chem. B* **2000**, *104*, 10549–10556.
(10) Pang, L.; Hwang, G. M.; Slutsky, B.; Fainman, Y. *Appl. Phys. Lett.* **2007**, *91*, 123112.
(11) Im, H.; Lesuffleur, A.; Lindquist, N. C.; Oh, S. H. *Anal. Chem.* **2009**, *81*, 2854–2859.
(12) Brolo, A. G.; Gordon, R.; Leathem, B.; Kavanagh, K. L. *Langmuir* **2004**, *20*, 4813–4815.
(13) Gordon, R.; Sinton, D.; Kavanagh, K. L.; Brolo, A. G. *Acc. Chem. Res.* **2008**, *41*, 1049–1057.
(14) Hwang, G. M.; Pang, L.; Mullen, E. H.; Fainman, Y. *IEEE Sens. J.* **2008**, *8*, 2074–2079.
(15) Malyarchuk, V.; Stewart, M. E.; Nuzzo, R. G.; Rogers, J. A. *Appl. Phys. Lett.* **2007**, *90*, 203113.
(16) Stewart, M. E.; Mack, N. H.; Malyarchuk, V.; Soares, J.; Lee, T. W.; Gray, S. K.; Nuzzo, R. G.; Rogers, J. A. *Proc. Natl. Acad. Sci. U.S.A.* **2006**, *103*, 17143–17148.
(17) Stewart, M. E.; Yao, J. M.; Maria, J.; Gray, S. K.; Rogers, J. A.; Nuzzo, R. G. *Anal. Chem.* **2009**, *81*, 5980–5989.
(18) Ji, J.; O'Connell, J. G.; Carter, D. J. D.; Larson, D. N. *Anal. Chem.* **2008**, *80*, 2491–2498.
(19) Hajiaboli, A. R.; Cui, B.; Kahrizi, M.; Truong, V. V. *Phys. Status Solidi A* **2009**, *206*, 976–979.
(20) Sinton, D.; Gordon, R.; Brolo, A. G. *Microfluid. Nanofluid.* **2008**, *4*, 107–116.
(21) Chen, J.; Shi, J.; Decanini, D.; Cambril, E.; Chen, Y.; Haghiri-Gosnet, A. M. *Microelectron. Eng.* **2009**, *86*, 632–635.
(22) Matsushita, T.; Nishikawa, T.; Yamashita, H.; Hasui, R.; Fujjita, S.; Okuno, Y. *Jpn. J. Appl. Phys.* **2008**, *47*, 7420–7427.
(23) Haynes, C. L.; Van Duyne, R. P. *J. Phys. Chem. B* **2001**, *105*, 5599–5611.
(24) Murray-Methot, M. P.; Menegazzo, N.; Masson, J. F. *Analyst* **2008**, *133*, 1714–1721.
(25) Cong, C. X.; Junus, W. C.; Shen, Z. X.; Yu, T. *Nanoscale Res. Lett.* **2009**, *4*, 1324–1328.
(26) Lee, S. H.; Bantz, K. C.; Lindquist, N. C.; Oh, S. H.; Haynes, C. L. *Langmuir* **2009**, *25*, 13685–13693.
(27) Li, H. Q.; Low, J.; Brown, K. S.; Wu, N. Q. *IEEE Sens. J.* **2008**, *8*, 880–884.
(28) Li, W.; Zhao, W.; Sun, P. *Physica E* **2009**, *41*, 1600–1603.
(29) Tan, B. J. Y.; Sow, C. H.; Koh, T. S.; Chin, K. C.; Wee, A. T. S.; Ong, C. K. *J. Phys. Chem. B* **2005**, *109*, 11100–11109.
(30) Yan, L. L.; Wang, K.; Wu, J. S.; Ye, L. *J. Phys. Chem. B* **2006**, *110*, 11241–11246.

(31) Zhang, Y.; Wang, X.; Wang, Y.; Liu, H.; Yang, J. *J. Alloys Compd.* **2008**, *452*, 473–477.
(32) Zhang, Y. J.; Li, W.; Chen, K. J. *J. Alloys Compd.* **2008**, *450*, 512–516.
(33) Huang, W. Y.; Qian, W.; El-Sayed, M. A. *Nano Lett.* **2004**, *4*, 1741–1747.
(34) Huang, W. Y.; Qian, W.; El-Sayed, M. A.; Ding, Y.; Wang, Z. L. *J. Phys. Chem. C* **2007**, *111*, 10751–10757.
(35) Willets, K. A.; Van Duyne, R. P. *Annu. Rev. Phys. Chem.* **2007**, *58*, 267–297.
(36) McFarland, A. D.; Van Duyne, R. P. *Nano Lett.* **2003**, *3*, 1057–1062.
(37) Live, L. S.; Masson, J. F. *J. Phys. Chem. C* **2009**, *113*, 10052–10060.
(38) Debruijn, H. E.; Altenburg, B. S. F.; Kooyman, R. P. H.; Greve, J. *Opt. Commun.* **1991**, *82*, 425–432.
(39) Sepúlveda, B.; Angelomé, P. C.; Lechuga, L. M.; Liz-Marzán, L. M. *Nano Today* **2009**, *4*, 244–251.
(40) Abdelghani, A.; Chovelon, J. M.; Krafft, J. M.; JaffrezicRenault, N.; Trouillet, A.; Veillas, C.; RonotTrioli, C.; Gagnaire, H. *Thin Solid Films* **1996**, *284*, 157–161.
(41) Ulman, A. *Chem. Rev.* **1996**, *96*, 1533–1554.
(42) Thio, T.; Ghaemi, H. F.; Lezec, H. J.; Wolff, P. A.; Ebbesen, T. W. *J. Opt. Soc. Am. B* **1999**, *16*, 1743–1748.
(43) Link, S.; Wang, Z. L.; El-Sayed, M. A. *J. Phys. Chem. B* **1999**, *103*, 3529–3533.
(44) Mallin, M. P.; Murphy, C. J. *Nano Lett.* **2002**, *2*, 1235–1237.
(45) Major, K. J.; De, C.; Obare, S. O. *Plasmonics* **2009**, *4*, 61–78.
(46) Ehler, T. T.; Noe, L. J. *Langmuir* **1995**, *11*, 4177–4179.
(47) Rodriguez-Gonzalez, B.; Burrows, A.; Watanabe, M.; Kiely, C. J.; Liz-Marzan, L. M. *J. Mater. Chem.* **2005**, *15*, 1755–1759.
(48) Stewart, M. E.; Anderton, C. R.; Thompson, L. B.; Maria, J.; Gray, S. K.; Rogers, J. A.; Nuzzo, R. G. *Chem. Rev.* **2008**, *108*, 494–521.
(49) Rindzevicius, T.; Alaverdyan, Y.; Dahlin, A.; Hook, F.; Sutherland, D. S.; Kall, M. *Nano Lett.* **2005**, *5*, 2335–2339.
(50) Dahlin, A. B.; Tegenfeldt, J. O.; Hook, F. *Anal. Chem.* **2006**, *78*, 4416–4423.
(51) Jonsson, M. P.; Jonsson, P.; Dahlin, A. B.; Hook, F. *Nano Lett.* **2007**, *7*, 3462–3468.
(52) Dahlin, A. B.; Jonsson, P.; Jonsson, M. P.; Schmid, E.; Zhou, Y.; Hook, F. *ACS Nano* **2008**, *2*, 2174–2182.
(53) De Leebeeck, A.; Kumar, L. K. S.; de Lange, V.; Sinton, D.; Gordon, R.; Brolo, A. G. *Anal. Chem.* **2007**, *79*, 4094–4100.
(54) Eftekhari, F.; Escobedo, C.; Ferreira, J.; Duan, X. B.; Girotto, E. M.; Brolo, A. G.; Gordon, R.; Sinton, D. *Anal. Chem.* **2009**, *81*, 4308–4311.
(55) Lesuffleur, A.; Im, H.; Lindquist, N. C.; Oh, S. H. *Appl. Phys. Lett.* **2007**, *90*, 243110.

JP101231C